AIAA SciTech Forum
9 - 13 January 2017, Grapevine, Texas
55th AIAA Aerospace Sciences Meeting

CrossMark
click for updates

Conceptual Design of a Man-Portable Ornithopter

Alex M. Moodie[1]
Andrew T. Gallaher[2]
Aviation Development Directorate
Aviation and Missile Research, Development, and Engineering Center
U.S. Army Aviation and Missile Command
Hampton, VA 23681; Moffett Field, CA 94035

Recent developments in avian-based flapping wing aircraft, or ornithopters, have demonstrated the potential for application as small unmanned aerial vehicles. This type of aircraft combines both maneuverability and high efficiency at low Reynolds numbers, leading to unique capabilities beyond traditional rotary-wing and fixed-wing aircraft. Additionally, mimicking the flight characteristics of avian species increases the difficulty of visual detection of the aircraft for intelligence, reconnaissance, and surveillance (ISR) roles. This study investigates the benefits and challenges of a hand launched, man-portable ornithopter UAS designed for an ISR mission. Conceptual designs of both an ornithopter and a fixed-wing aircraft are performed and comparisons of weight and performance are made.

Nomenclature

A	=	propeller disk area	$P_{installed}$	=	installed power
AR	=	wing aspect ratio	SDGW	=	structural design gross weight
b	=	wing span	S_{ref}	=	wing projected area
bfold	=	folded wing span fraction	S_{wet}	=	fuselage wetted area
C	=	discharge capacity	t	=	time
CF	=	cost function	T	=	thrust
D	=	diameter	TR	=	taper ratio
dy	=	wing strip span-wise width	U_∞	=	free stream velocity
e	=	ratio of extended to retracted wing span	WE	=	weight empty
f	=	flap frequency	WMTO	=	maximum takeoff weight
f_Q	=	second rotor toque limit, %	y	=	span-wise distance to wing strip
GW	=	gross weight	D/q	=	equivalent drag area
ISA	=	international standard atmosphere	L/De	=	equivalent lift to drag ratio
L	=	length	t/c	=	wing thickness to chord ratio
mAh	=	milliamp-hours	α_0	=	zero lift angle of attack
N_{cell}	=	number of battery cells	β_0	=	wing twist amplitude
N_{gb}	=	number of gear boxes	ϕ	=	propeller pitch
n_w	=	number of wing strips	γ_0	=	wing flap amplitude
nz	=	load factor	Λ	=	wing sweep angle
nz_{ult}	=	ultimate load factor	θ_0	=	wing root pitch amplitude
P	=	power	Ω	=	propeller rotational speed
P_{DS}	=	drive system output power	ζ	=	phase angle

[1] Aerospace Engineer

[2] Aerospace Engineer

This material is declared a work of the U.S. Government and is not subject to copyright protection in the United States.
DISTRIBUTION STATEMENT A: Approved for public release; distribution is unlimited.

This material is declared a work of the U.S. Government and is not subject to copyright protection in the United States.

Downloaded by UNIVERSITY OF COLORADO on January 11, 2017 | http://arc.aiaa.org | DOI: 10.2514/6.2017-0013

Downloaded by UNIVERSITY OF COLORADO on January 11, 2017 | http://arc.aiaa.org | DOI: 10.2514/6.2017-0013

I. Introduction

The last decade has seen unprecedented worldwide proliferation of unmanned flying aircraft, commonly referred to as "drones", in both the civilian and military spheres. The vast majority of these aircraft types are based on conventional modes of thrust and lift generation (e.g. rotors, propellers and wings). The concept of building a bird-like flying machine dates as far back as Leonardo DaVinci; with the first flying rubber band powered models developed by Alphonse Pénaud in the 1870's. Recent developments in flapping wing concepts has reinvigorated the pursuit of biologically inspired flight [1-13]. Avian species have been extensively studied to gain an understanding of the mechanics of bird flight [14-17]. An understanding of this avian wing gait has led to the development of engineering models to aid designers of aircraft with this method of locomotion [18-20].

Emerging military needs are migrating towards significant increases in autonomy, range, and endurance; while maintaining a desire for these increased capabilities to be packaged in smaller and lower-cost aircraft solutions [21]. The research of aircraft platforms capable of performing roles and missions within the man-portable size class that employ flapping wings for locomotion has been largely focused on Micro Air Vehicles (MAV) [22]. An avian-based flapping wing aircraft has the potential to augment or compete with the RQ-11 Raven, while providing improved aircraft survivability at shorter standoff ranges when compared to a propeller driven fixed wing aircraft. The focus of this study is the development of a conceptual design of a flapping-wing aircraft, or ornithopter, and to make comparisons to a fixed wing counterpart.

II. Approach

A reference performance specification is developed to provide objectives and constraints to the conceptual design process. Included in this performance specification are: payload, combat radius, endurance, operating conditions, gross weight, geometric limitations, and methods of launch and retrieval. For the purposes of this study, the values of these requirements are based on the current capability of the RQ-11 Raven. To size the aircraft, the combination of payload, combat radius, endurance and operating conditions are represented in a flight profile, shown in Figure 1. No ground support equipment or improved surface can be considered to launch and recover the aircraft. In essence, the aircraft must be able to be strapped to a rucksack and either have vertical takeoff and landing (VTOL) capability or be hand-launched. The requirements described above are shown in Table 1 for clarity.

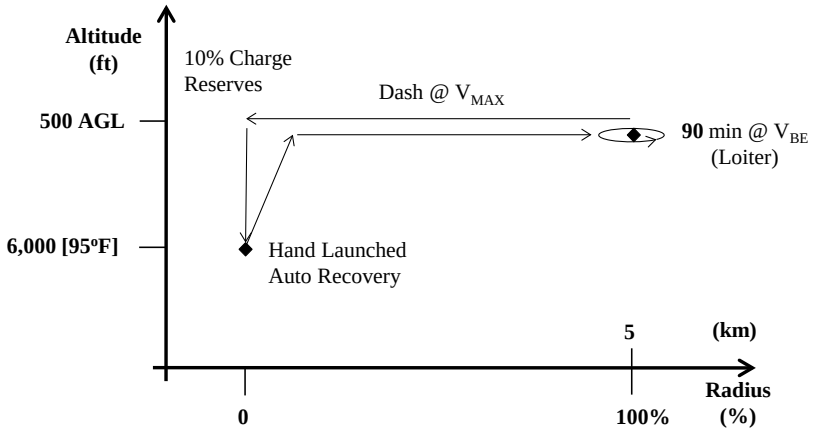

Figure 1. Aircraft Sizing Flight Profile

Table 1. Summary of Design Requirements

	Description	Value
Payload	EO/IR Sensor	0.3 lb
Combat Radius	Distance to Target	5 km
Time on Station	Flight Endurance over Target	90 min
Flight Condition	Altitude and Temperature	6,000ft, 95F
Launch & Retrieve	Hand Launch, Auto Recovery	-
Maximum Gross Weight	-	6 lb
Maximum Operating Length	-	4.5 ft
Maximum Operating Width	-	6.75 ft

Downloaded by UNIVERSITY OF COLORADO on January 11, 2017 | http://arc.aiaa.org | DOI: 10.2514/6.2017-0013

AIRCRAFT WEIGHT

The aircraft empty weight is a buildup of component weights. The primary components considered for this study are based on the Group Weight Statement, defined in Ref 23. Each component is either a fixed estimate or a scaled estimate. Scaled component weight models are developed to capture the scaling effects related to key design parameters. A list of the component weights and whether they are treated as fixed or scaled estimates is presented in Table 2.

Table 2. Aircraft Empty Weight Components

Wing	Scaled
Rotor	Scaled
Tail	Scaled
Body	Scaled
Alighting Gear	Fixed
Propulsion	Scaled
Flight Controls	Fixed
Electrical	Fixed
Avionics	Fixed
Battery	Scaled

WING

The wing weight equation is taken from Ref. 24 and is shown below.

$$W_{Wing} = 5.66411 * \left(\frac{SDGW}{1{,}000 * \cos(\Lambda)}\right)^{0.874} * nz^{0.39579} * {S_{ref}}^{0.21754} * AR^{0.50016} * \left(\frac{1+TR}{t/c}\right)^{0.09359} * (1 - b_{fold})^{-0.14356}$$

Where the SDGW is assumed to be the same as the DGW, nz is assumed to be 6 g, and b_{fold} is zero. The primary factors driving the wing weight are the weight of the aircraft, aspect ratio, load factor, and wing area. For the ornithopter wing, an additional 10% is added to the wing weight to account for the twisting motion, which likely means a circular spar with floating or controlled ribs.

PROPELLER

The propeller weight equation, shown below, is based on a linear regression of 150 small propellers, available in the consumer market.

$$W_{Propellor} = 0.00177 * D^{2.57329} * \phi^{0.48293} * {N_b}^{3.16944}$$

Where D is the propeller diameter, ϕ is the distance the propeller move in one revolution and N_b is the number of blades. The error in the predicted weight for each of the 150 propellers considered is presented in Figure 2. The average error for this linear regression is 27.8% and the R^2 is 0.973, with the highest scatter for the smaller size propellers. The actual vs predicted motor weight is presented in Figure 3 along with 80% confidence lines.

TAIL

The tail weight equation is taken from the horizontal tail model in Ref. 24 and is shown below.

$$W_{ht} = 0.7176 * {S_{ref}}^{1.1881} * AR^{0.3173}$$

Both the ornithopter and the fixed wing tails are sized by assuming a tail volume of 0.01, based on the wing area and chord and tail span.

BODY

The body weight scaling equation is taken from Ref. 24 and is shown below.

$$W_{body} = 25.41 * \left(\frac{WMTO}{1{,}000}\right)^{0.4879} * \left(nz_{ult} * \frac{SDGW}{1{,}000}\right)^{0.2075} * {S_{wet}}^{0.1676} * L^{0.1512}$$

Where the WMTO and SDGW are assumed to equal the DGW and nz_{ult} is 5.25 g. The body S_{wet} and length for the ornithopter is determined by a CAD model, shown below in Figure 22, and by a streamlined shape similar in size the RQ-11 fuselage.

PROPULSION

The propulsion group is sub-divided into three components for this study: electric motor, electronic speed control (ECS), and drive. The electric motor weight model is based on a linear regression of 605 small electric motors, available in the consumer market.

$$W_{Motor} = 1.339 * \left(\frac{RPM}{1{,}000}\right)^{-0.293} * P^{0.827} * \left(\frac{L}{D}\right)^{0.336}$$

Where P is the motor peak power in Watts and L/D is the ratio of the motor length to diameter. The average L/D for the dataset is 1.6, which is assumed for this study. The error in the predicted weight for each motor in the data set is presented in Figure 4. The average error is 27.9% and the R^2 is 0.857, with significant scatter for the smaller size motors. There also is a sloping trend in the error, which may indicate dependence on another parameter, not available in the data set. The actual vs predicted motor weight is presented in Figure 5 along with 80% confidence lines.

The weight of the electronic speed control is based on a linear regression of 44 models available in the consumer market. The weight is assumed to be primarily driven by the motor amperage, resulting in the following relationship:

$$W_{ecs} = 2.998 * Amps^{0.863}$$

The error in the predicted weight for each electronic speed control in the data set is presented in Figure 6. The average error is 31.9% and the R^2 is 0.78. The actual vs predicted motor weight is presented in Figure 7 along with 80% confidence lines.

The weight of the flapping drive mechanism for the ornithopter is assumed to analogous to the transmission of a helicopter, in that the weight is primarily driven by torque and the difference between the input and output RPM. Therefore, the scaling weight equation is taken from Ref. 24, shown below.

$$W_{drive} = 57.72 * {P_{DS}}^{0.8195} * {f_Q}^{0.068} * {N_{gb}}^{0.0663} * \frac{\left(\frac{RPM_{Motor}}{1{,}000}\right)^{0.0369}}{{RPM_{Rotor}}^{0.6379}}$$

Where PDS is the power required at the output of the drive, fQ and Ngb are set to 1, RPM_{motor} is the input RPM and RPM_{rotor} is the output RPM. For the fixed wing design, it is assumed that the propeller is mounted directly to the motor shaft, therefore no drive weight is included.

The mechanism conceived for this study is based on gears and linkages to generate the sinusoidal motion of the wing. An alternative approach is to develop actuators for each motion, similar to a bird's wing. While this certainly increases the complexity of the wing controller, adjustments of the wing gait could be made that wouldn't be practical for a mechanical system, such as converting from a sinusoidal motion to a square wave-like motion. This alternative approach also has an added benefit of allowing for control over the wing motion when the aircraft is gliding; to compensate for gusts and improve maneuverability, as examples.

FIXED WEIGHTS

The alighting gear, flight controls, electrical system, and avionics are all assumed to be fixed for this study. A deeper investigation of the relationship of these component weights to design and/or mission parameters may yield scaling functions, however this work is beyond the scope of the current study. The weight of the flight control system is based on four micro servos for the fixed wing design and ten micro servos for the ornithopter design, weighing 0.02 lb each. The avionics weight is assumed to be 1 lb. The electrical system and instruments weight are assumed to each be 0.5% of the DGW.

BATTERY WEIGHT

The battery weight model is based on a linear regression of 1,058 batteries available in the consumer market, specifically for remote controlled vehicles.

$$W_{Battery} = 0.028 * {N_{cell}}^{0.976} * mAh^{0.949} * C^{0.12}$$

Downloaded by UNIVERSITY OF COLORADO on January 11, 2017 | http://arc.aiaa.org | DOI: 10.2514/6.2017-0013

Where N_{cell} is the number of cells in series, mAh is the battery capacity and C is the discharge capacity of the battery. The error in the predicted battery weight is presented in Figure 8. The average error is 5.72% and the R^2 is 0.99, showing good agreement at the larger sizes and increasing scatter as the batteries scale down. The actual vs predicted weight is shown in Figure 9, along with 80% confidence lines.

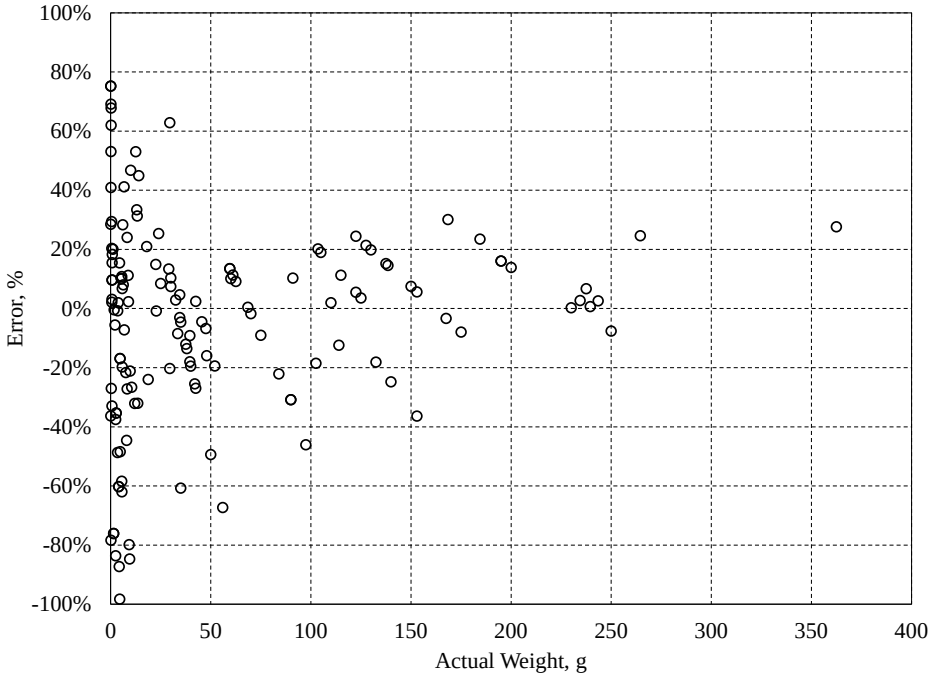

Figure 2. Propeller Weight Model Error

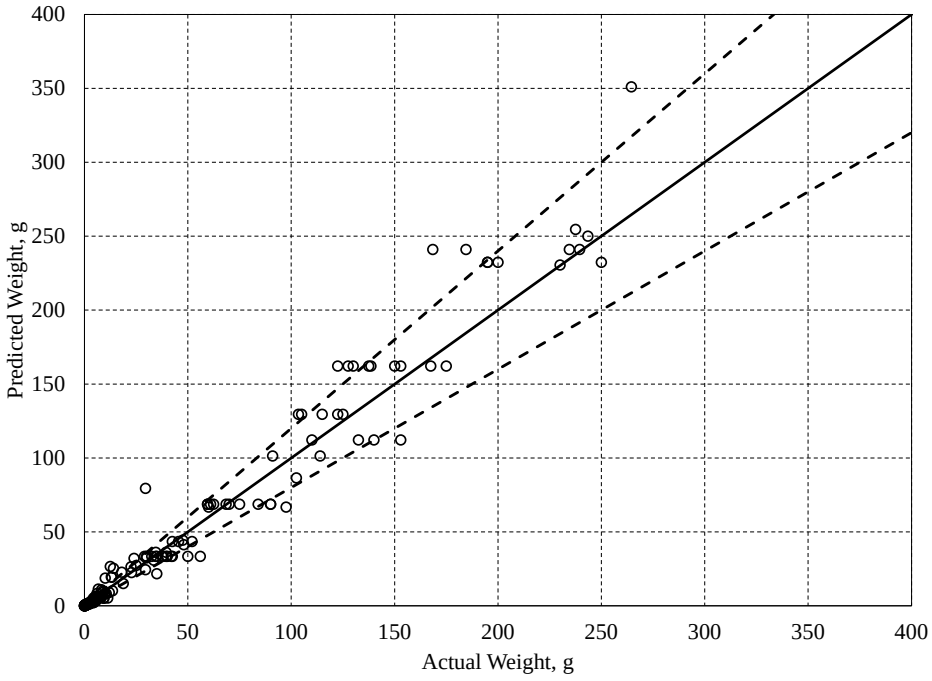

Figure 3. Propeller Actual vs Predicted Weight with 80% Confidence Lines

Downloaded by UNIVERSITY OF COLORADO on January 11, 2017 | http://arc.aiaa.org | DOI: 10.2514/6.2017-0013

Downloaded by UNIVERSITY OF COLORADO on January 11, 2017 | http://arc.aiaa.org | DOI: 10.2514/6.2017-0013

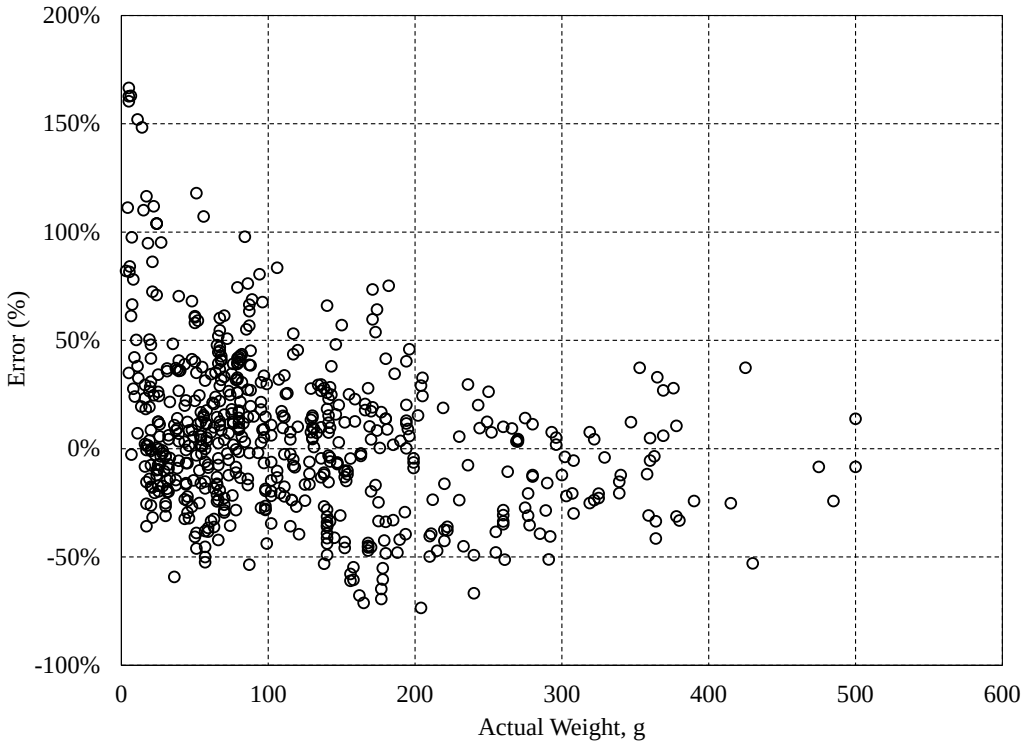

Figure 4. Electric Motor Weight Model Error

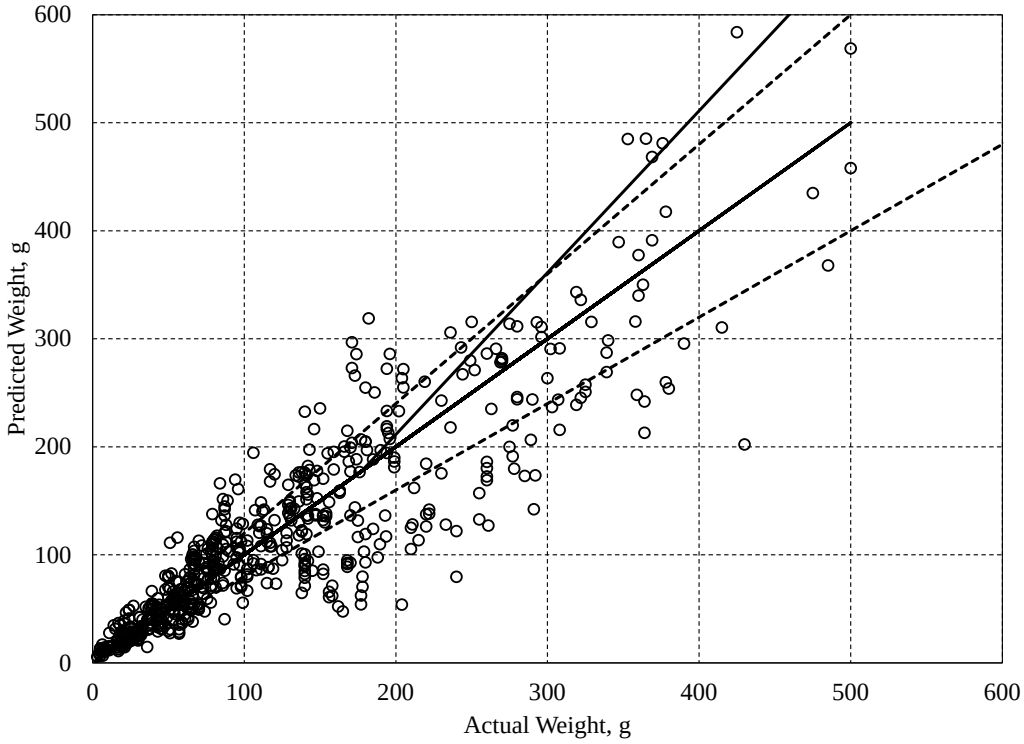

Figure 5. Electric Motor Actual vs Predicted Weight with 80% Confidence Lines

Downloaded by UNIVERSITY OF COLORADO on January 11, 2017 | http://arc.aiaa.org | DOI: 10.2514/6.2017-0013

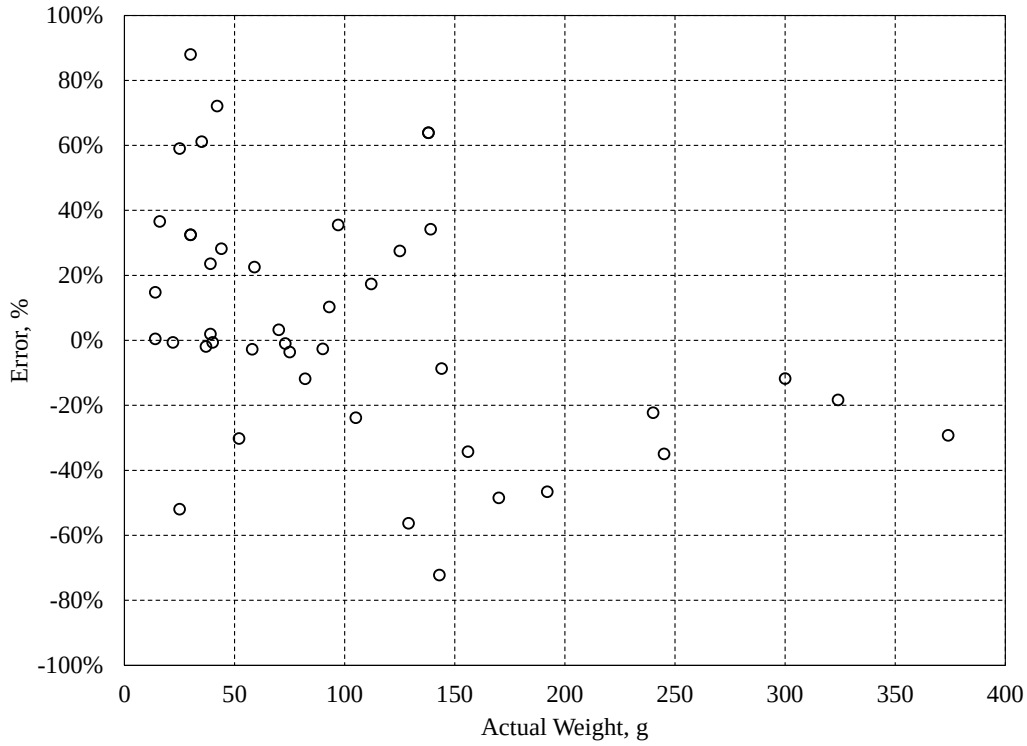

Figure 6. ECS Weight Model Error

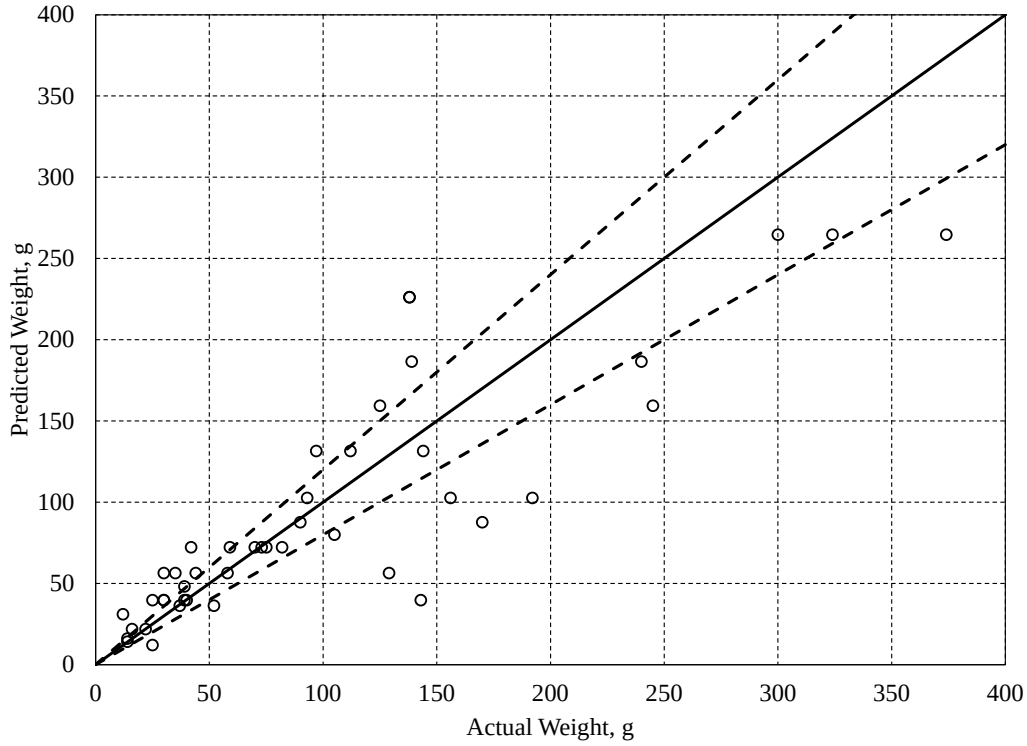

Figure 7. ECS Actual by Predicted Weight with 80% Confidence Lines

Downloaded by UNIVERSITY OF COLORADO on January 11, 2017 | http://arc.aiaa.org | DOI: 10.2514/6.2017-0013

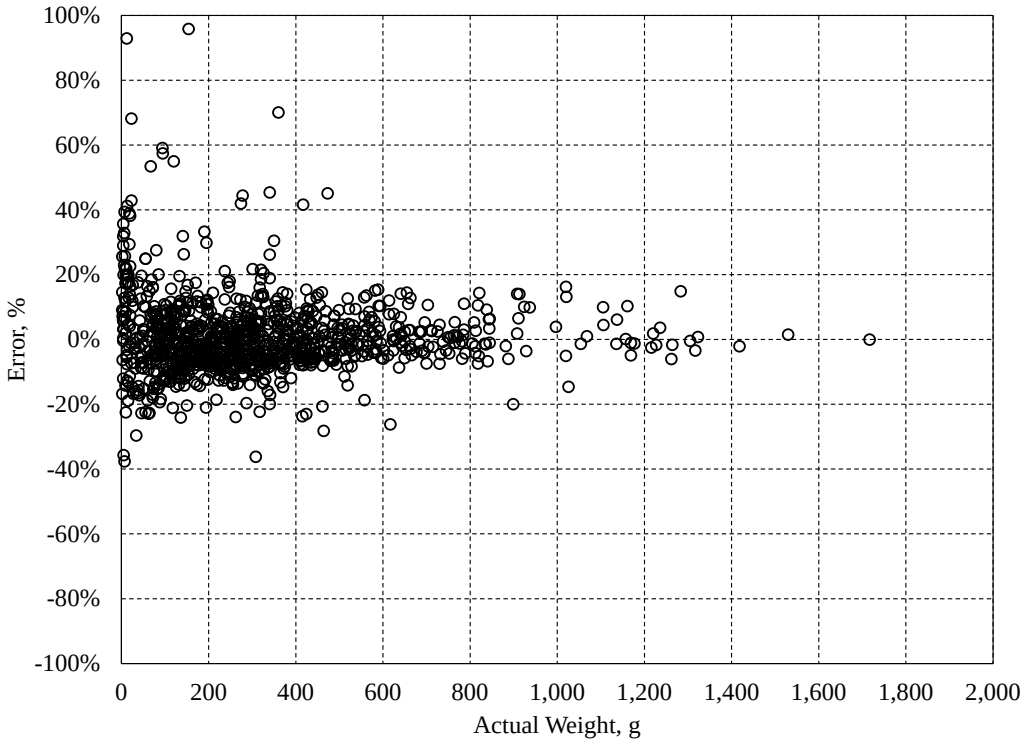

Figure 8. Battery Weight Model Error

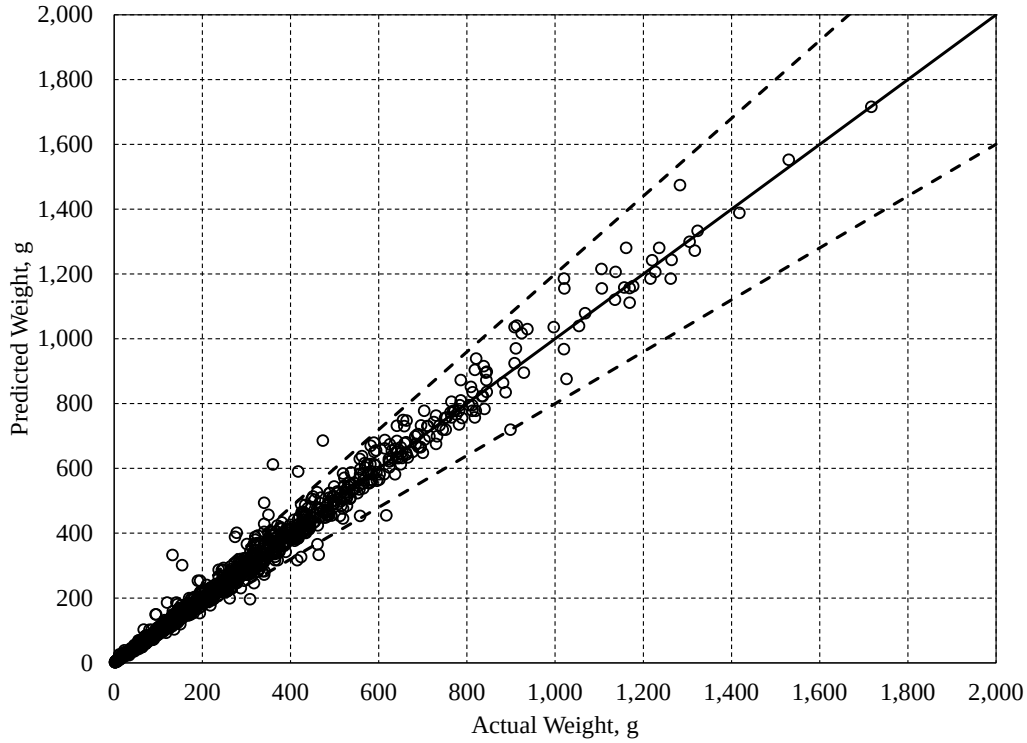

Figure 9. Battery Actual by Predicted Weight with 80% Confidence Lines

FIXED WING PERFORMANCE MODEL

The wing aerodynamic model for the fixed aircraft is based on the lifting line model by Anderson [25]. The airfoil used for this wing is the Drela AG12, which has good L/D characteristics at low Reynolds numbers [26]. Similar to the ornithopter, the wing has an elliptical planform, with an aspect ratio of 14 and wing loading equal to 1.75 lb/sq.ft. The isolated wing lift-to-drag ratio (L/D) as a function of lift coefficient (Cl) is shown in Figure 10.

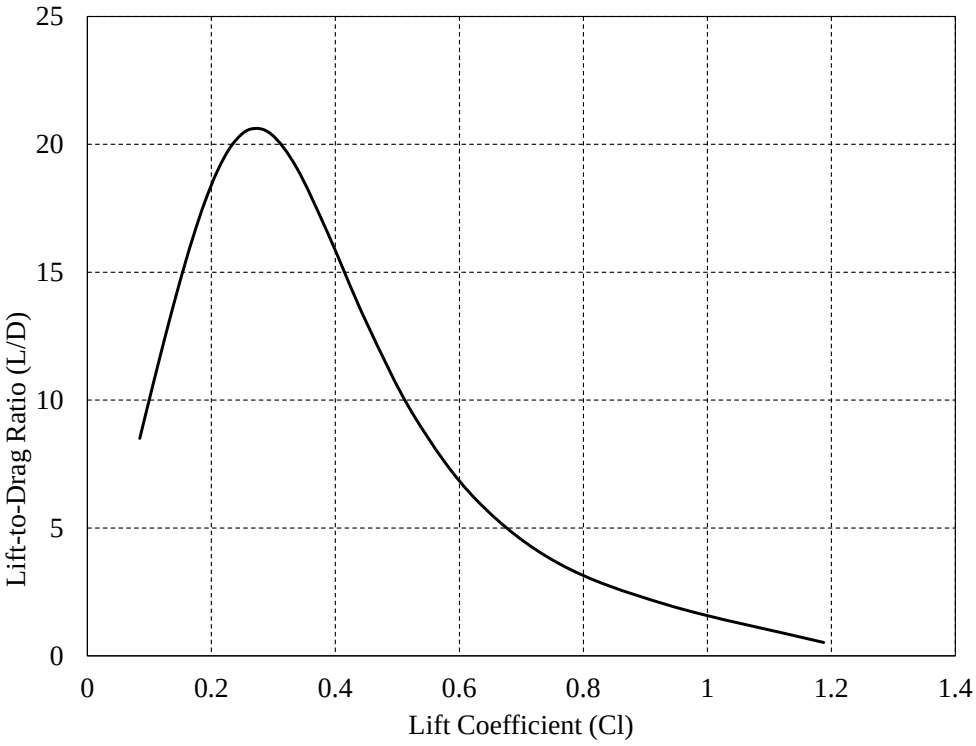

Figure 10. Wing Lift-to-Drag Ratio as a Function of Lift Coefficient

The reduced order model of a propeller is taken from Johnson [24] and calibrated to an APC 8X6 propeller tested by Brandt and Selig [27]. A comparison of the propeller model to the test data is presented in Figure 11. The power and thrust coefficients for the propeller are defined below.

$$C_T = \frac{T}{\rho A \left(\Omega \frac{\mathrm{D}}{2}\right)^2}$$

$$C_P = \frac{P}{\rho A \left(\Omega \frac{\mathrm{D}}{2}\right)^3}$$

Where ρ is the air density, A is the propeller disk area, Ω is the propeller rotational speed, and R is the propeller radius.

Downloaded by UNIVERSITY OF COLORADO on January 11, 2017 | http://arc.aiaa.org | DOI: 10.2514/6.2017-0013

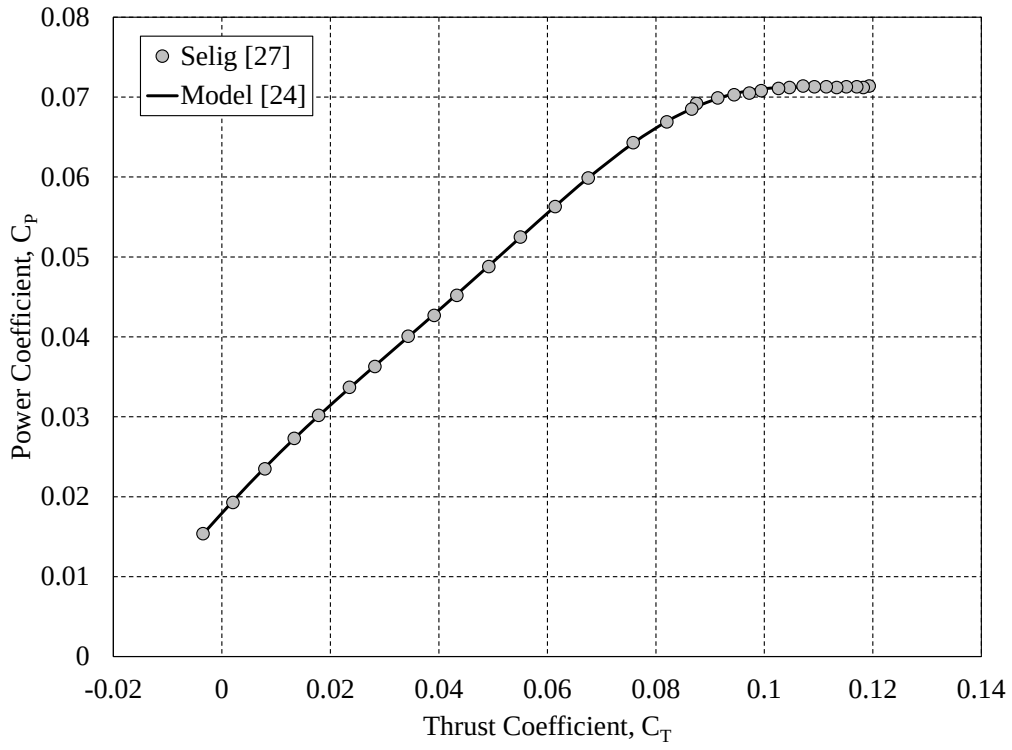

Figure 11. Propeller Power as a Function of Thrust

ORNITHOPTER PERFORMANCE MODEL

The two unique aspects of an ornithopter design are the mechanism to accomplish the wing motion, and wing motion itself. The mechanical efficiency and space claim of the mechanism are derived from the work of Räbiger [12]. An aerodynamic strip theory based performance model of a wing undergoing harmonic flapping, pitching, and twisting motion is taken from DeLaurier [18] and assumes the wing has an elliptical chord distribution and constant airfoil cross section with the Drela AG12 airfoil [26]. Additionally, this model is modified to handle additional wing extension and retraction degrees of freedom, based on Parslew [20]. The harmonic motions of the wing are defined in the following equations, with the angles defined in Figure 12. The harmonic wing motion is shown in Figure 13 depicting the wing pitch and twist for both the down-stoke and up-stroke.

Flapping Motion:

$$\gamma = \gamma_0 \cos(2\pi f t)$$

Pitching Motion:

$$\theta = -\theta_0 \cos(2\pi f t + \zeta)$$

Twisting Motion:

$$\beta(y) = -\beta_0 y \cos(2\pi f t + \zeta)$$

Extension/Retraction Motion:

$$dy = \begin{cases} b/(2 \cdot n_w), & \dot{\gamma} < 0 \quad (down - stroke) \\ b/(2 \cdot n_w) \cdot (1 - (1 - e) \cdot \cos(2\pi f t + \zeta)), & \dot{\gamma} > 0 \quad (up - stroke) \end{cases}$$

Downloaded by UNIVERSITY OF COLORADO on January 11, 2017 | http://arc.aiaa.org | DOI: 10.2514/6.2017-0013

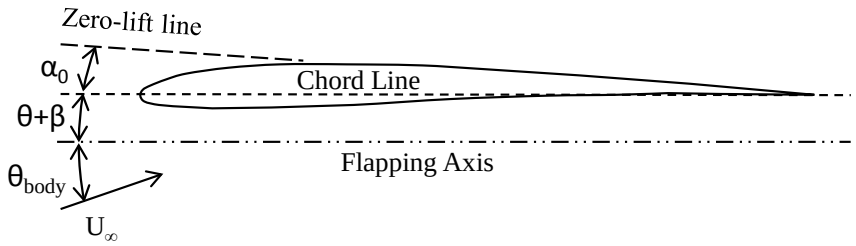

Figure 12. Wing Strip Angle Definitions

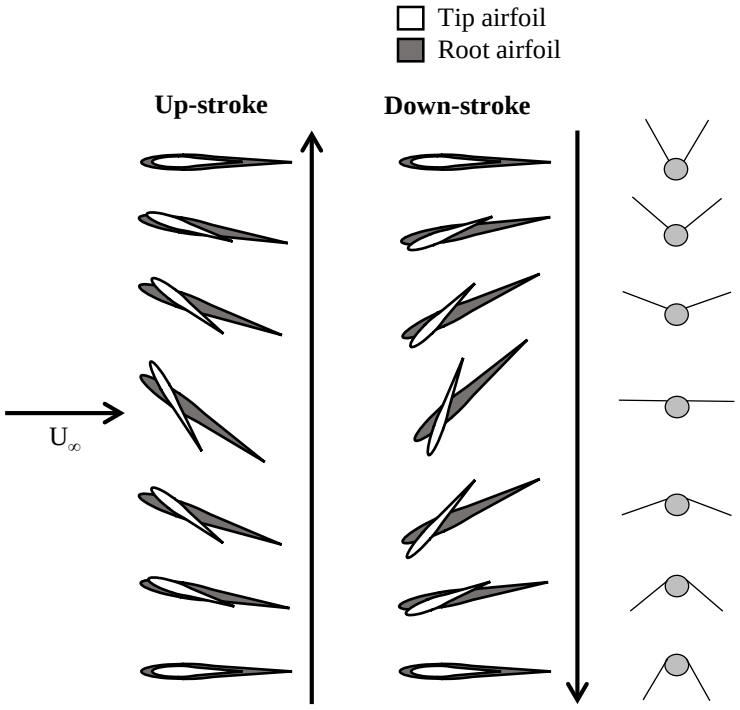

Figure 13. Harmonic Wing Pitch and Twist Motion

III. Results

With consideration of these four wing motions and the wing flap frequency, there are five independent variables to control the lift and thrust in steady flight. To gain a better understanding of the characteristics each of these motions has on the performance of the flapping wing a series of parameter sweeps are performed for flapping, wing root pitch, twist, and extension/retraction fraction, shown in the figures below.

Overall the wing twist and root pitch show the largest impact on the aircraft performance, with extension/retraction showing the least variability. Therefore, for this study the wing extension/retraction motion is not considered in the overall design. It is apparent from these parameter sweeps that there are boundaries to the maximum and minimum half amplitude angles, driven largely by stall. In addition to poor performance, the stability of the current algorithm begins to degrade when these boundaries are exceeded. The following figures show the upper and lower bounds of the half amplitude angles for flap, wing root pitch and wing twist over a range of airspeeds. Additionally, the combination of flap, wing root pitch and wing twist that gives the peak aerodynamic efficiency (L/De) is estimated using a coordinate pattern search.

Downloaded by UNIVERSITY OF COLORADO on January 11, 2017 | http://arc.aiaa.org | DOI: 10.2514/6.2017-0013

Downloaded by UNIVERSITY OF COLORADO on January 11, 2017 | http://arc.aiaa.org | DOI: 10.2514/6.2017-0013

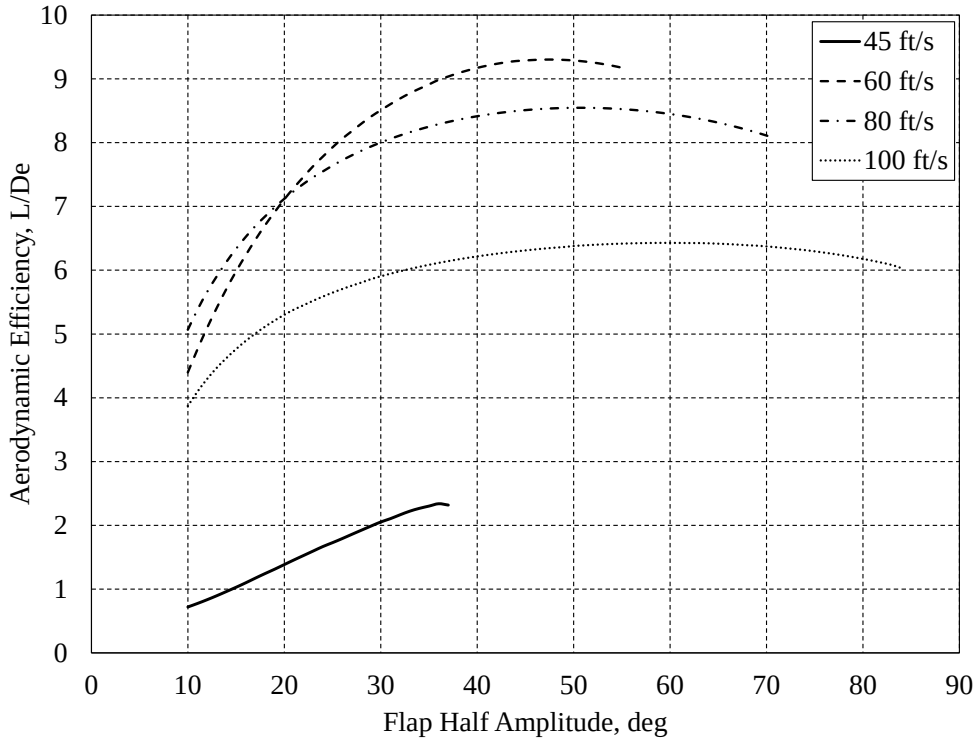

Figure 14. Aerodynamic Efficiency as a Function Wing Flap Half Amplitude for Airspeeds of 45, 60, 80, and 100 ft/s, and Peak Root Pitch and Twist as Shown in Figs. 19-20,

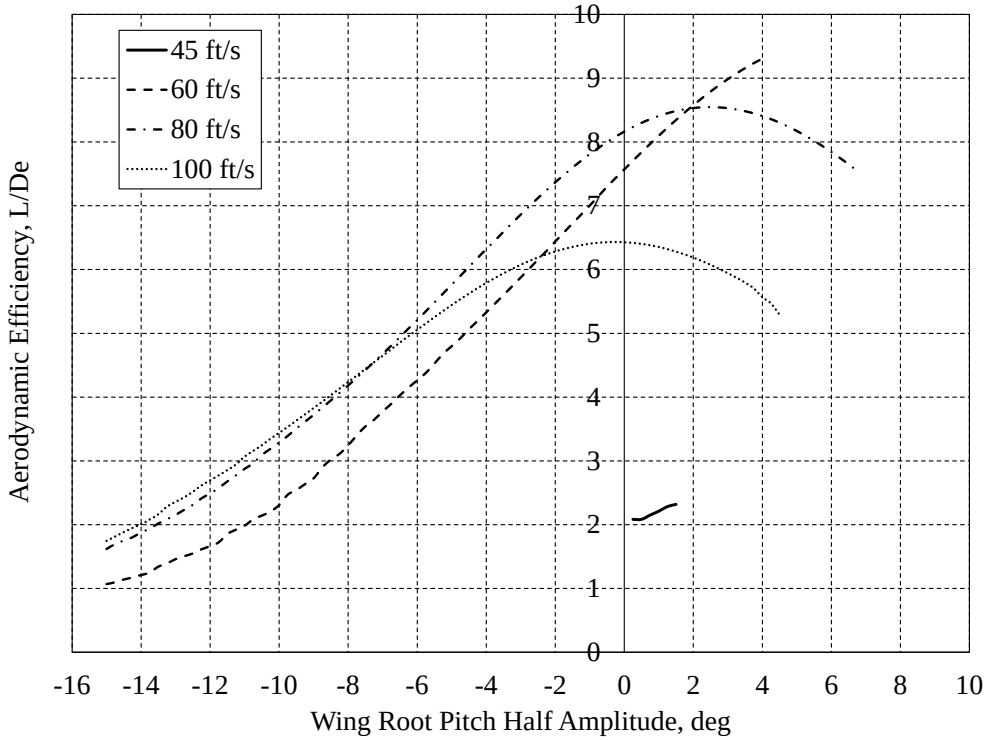

Figure 15. Aerodynamic Efficiency as a Function Wing Root Pitch Half Amplitude for Airspeed of 45, 60, 80, and 100 ft/s, and Peak Flap and Twist as Shown in Figs. 18 and 20

Downloaded by UNIVERSITY OF COLORADO on January 11, 2017 | http://arc.aiaa.org | DOI: 10.2514/6.2017-0013

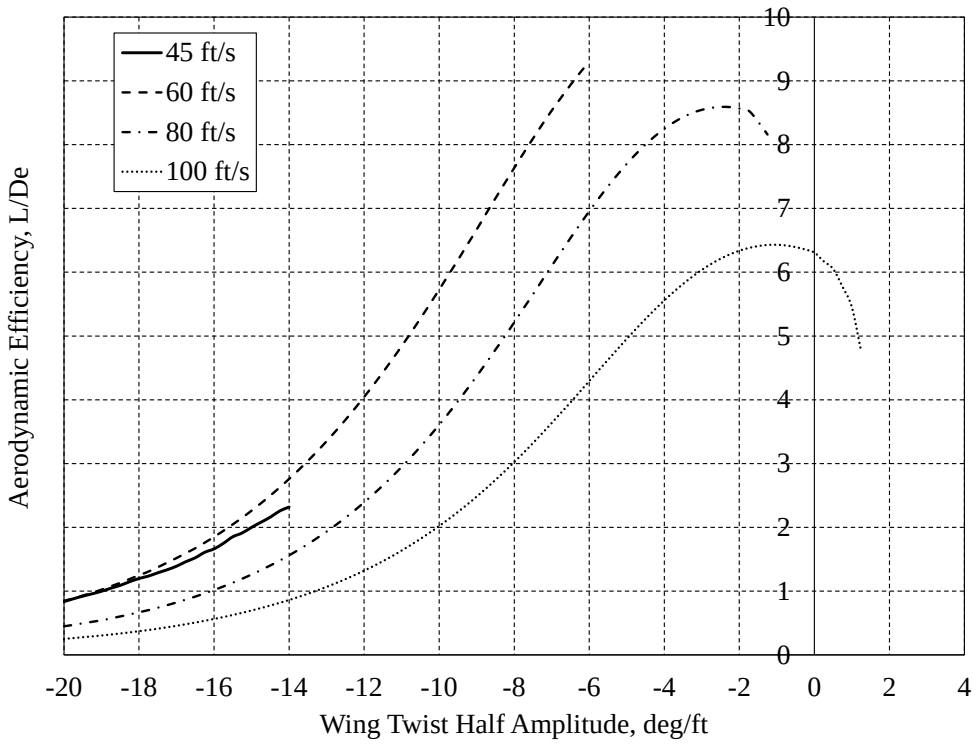

Figure 16. Aerodynamic Efficiency as a Function Wing Twist Half Amplitude for Airspeed of 45, 60, 80, and 100 ft/s, and Peak Flap and Root Pitch as Shown in Figs. 18-19

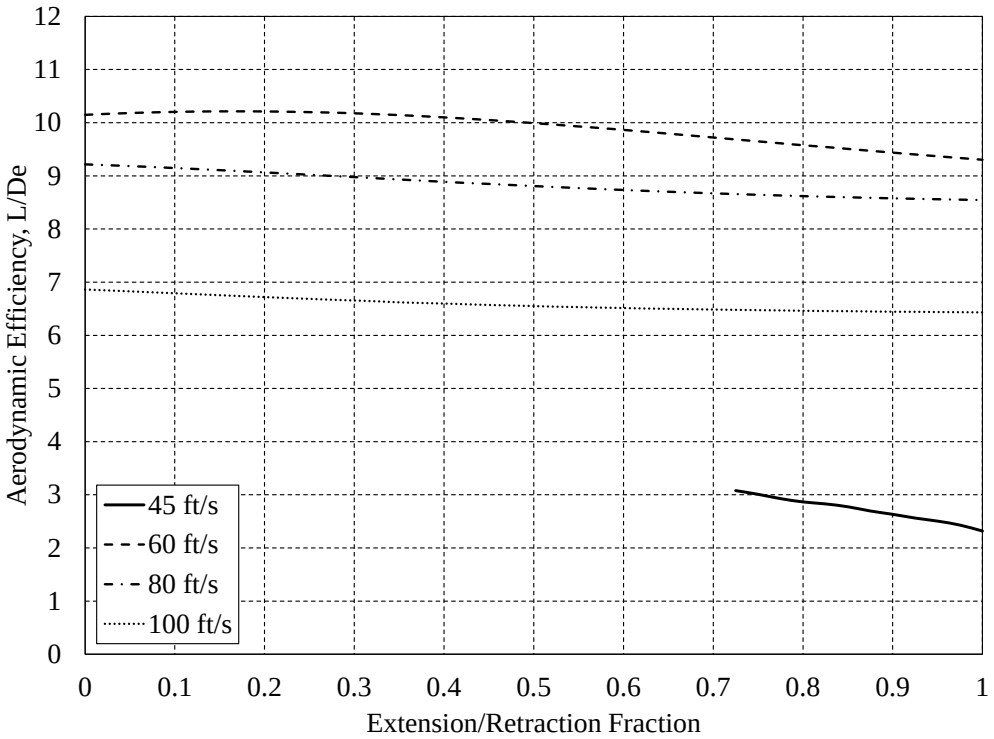

Figure 17. Aerodynamic Efficiency as a Function Wing Extension/Retraction Fraction for Airspeed of 45, 60, 80, and 100 ft/s, and Peak Flap, Root Pitch and Twist as Shown in Figs. 18-20

Downloaded by UNIVERSITY OF COLORADO on January 11, 2017 | http://arc.aiaa.org | DOI: 10.2514/6.2017-0013

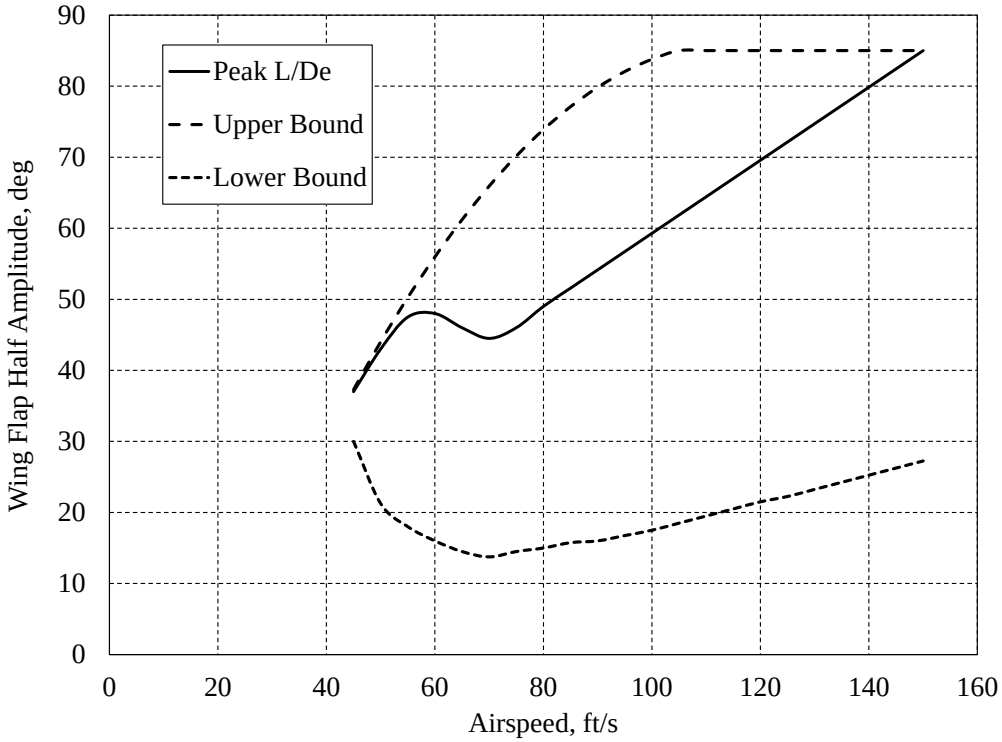

Figure 18. Wing Flap Half Amplitude Bounds and Peak as a Function of Airspeed for Peak Root Pitch and Twist as Shown in Figs. 19-20

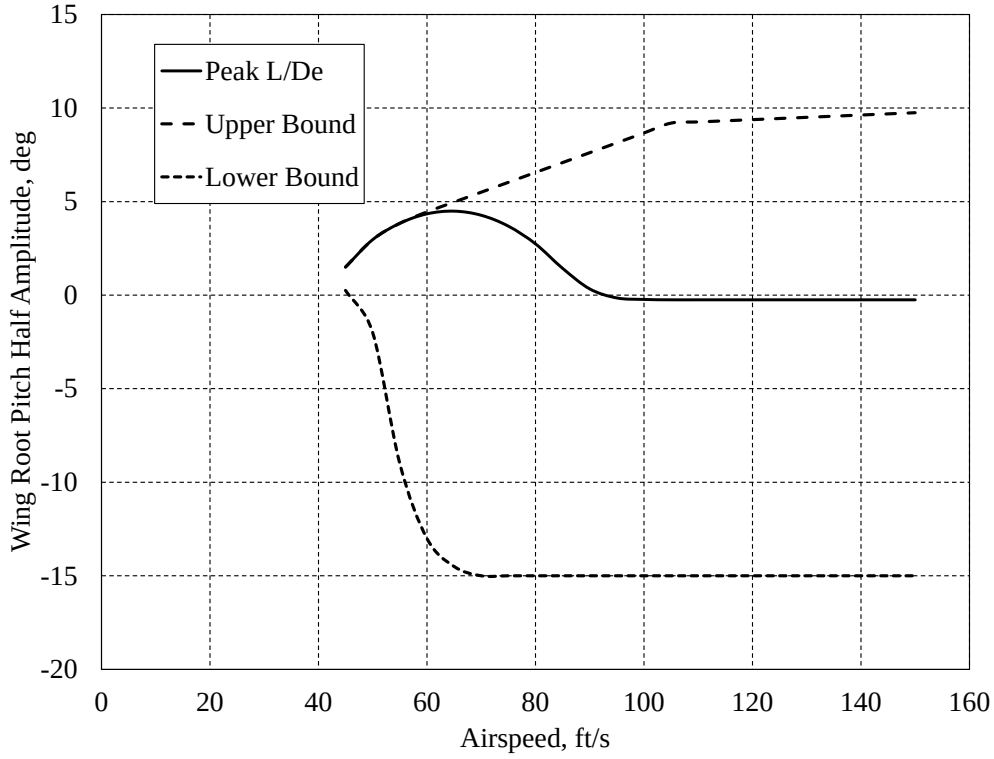

Figure 19. Wing Root Harmonic Pitch Half Amplitude Bounds and Peak as a Function of Airspeed for Peak Flap and Twist as Shown in Figs. 18 and 20

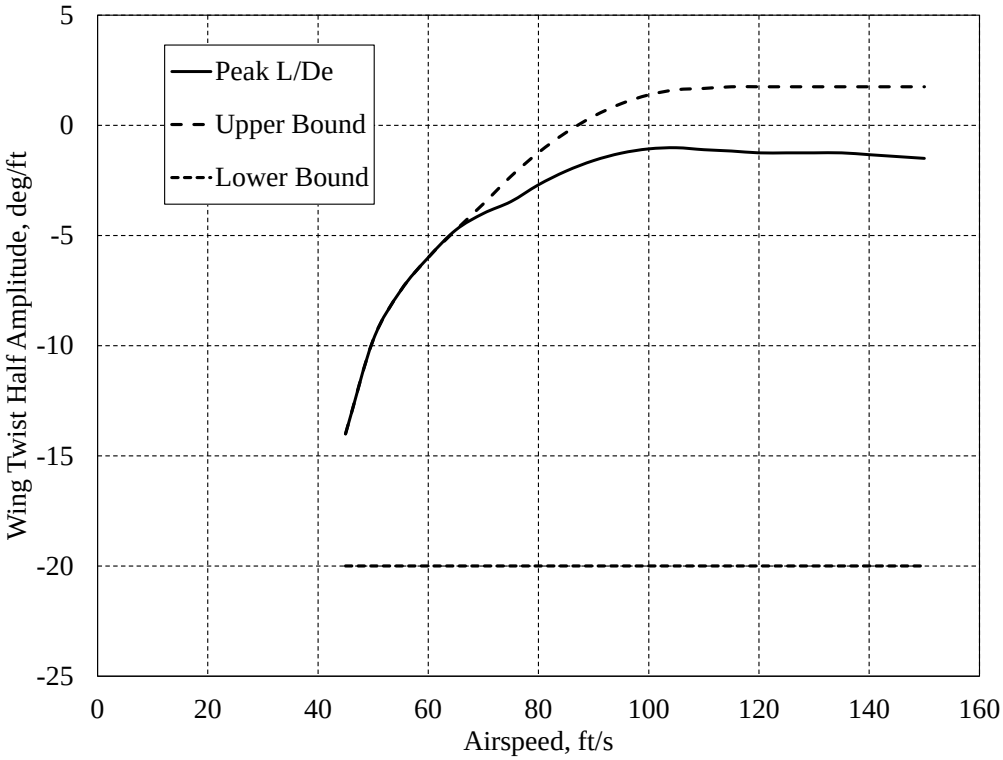

Figure 20. Wing Harmonic Twist Half Amplitude Bounds and Peak as a Function of Airspeed for Peak Flap and Root Pitch as Shown in Figs. 18-19

The flap motion is assumed to be constrained based on considerations such as flap frequency limits and wing-body mechanical interference, respectively. As the flap angle is reduced, the flap frequency must be increased to maintain trim. An upper limit on flap frequency of 4 Hz is assumed for this study, which dictates the shape of the lower boundary. The upper bound follows the wing stall limit until it hits the assumed mechanical limit of 85 degrees half amplitude for speeds in excess of 100 ft/s. Below 45 ft/s the wing is stalled and no steady flight trim solution could be found. It's notable that the flap angle boundaries converge as the speed decreases. This behavior is thought to be influenced by the motion of the wing, which in this case is sinusoidal. Similar to the flapping, the wing root pitching motion shows a very small range of acceptable angles at the low end of the airspeed range. However, the boundaries quickly diverge as speed increases. The upper and lower limits to the boundaries are assumed to be +-15 degrees, based on the difficulty to pitch the wing root and tip concurrently in the small space available at the wing-body attachment. The total angle assumed is +-75 degrees, root pitch plus tip pitch for 20 degrees/ft twist. The wing twist for peak aerodynamic efficiency shows a tendency to follow the upper boundary, which causes some difficulty for the optimizer. By identifying the boundaries and incorporating them as constraints in the optimization, the model showed marked improvements in convergence and run time, especially at lower airspeeds.

In order to determine the wing planform, a design point of 60 ft/s at 6,500 ft and 95F is selected, the wing aspect ratio and wing loading are then varied to find the combination with the lowest cost function, CF, as defined in Ref 28, and shown below.

$$CF = WE^{0.4854} * P_{Installed}{}^{0.5843}$$

At wing loadings greater than 1.5 – 2 lb/sq.ft. the wing performance drops off very quickly due to the onset of stall, driving the aircraft size, installed power, and resulting cost function upward. For wing loadings lighter than 1 lb/sq.ft. the inertial power, a result of increased wing weight, begins to dominate the installed power and compounds with the increasing wing weight to drive the cost function up. The cost function begins to plateau at a wing aspect ratio of 14, due to the increased wing weight. A wing loading of 1.75 and aspect ratio of 14 are selected for this design study.

Downloaded by UNIVERSITY OF COLORADO on January 11, 2017 | http://arc.aiaa.org | DOI: 10.2514/6.2017-0013

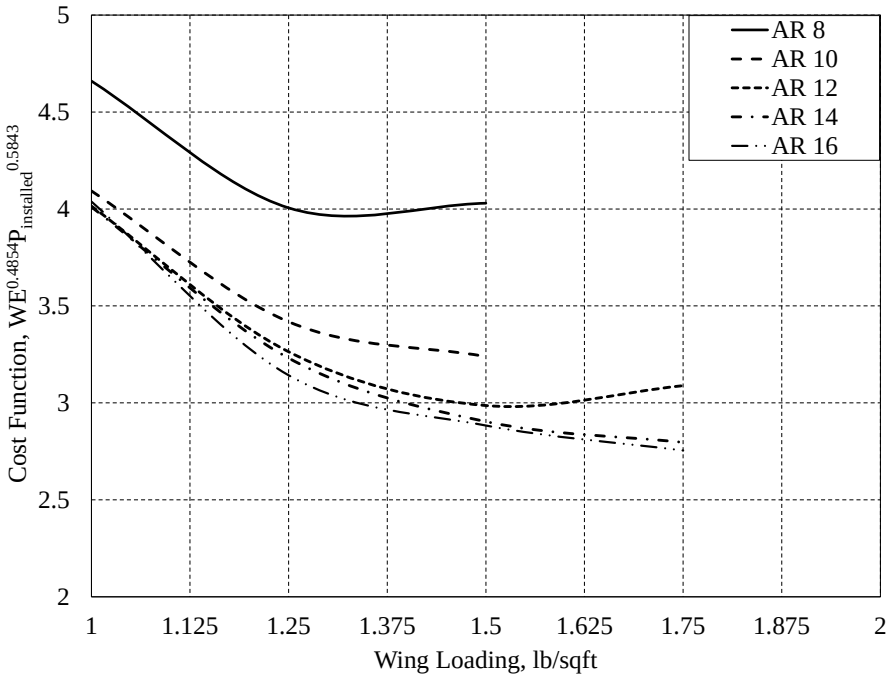

Figure 21. Cost Function vs. Wing Loading for Wing Aspect Ratios Ranging from 8 to 16

The results of the mission are presented in Table 3 and Table 4, showing the airspeed, flight time and energy consumption for each segment of the mission. The total mission energy consumption determines the battery size. For the ornithopter, the electric motor is sized to meet the peak power requirement during the flap cycle at the cruise condition of 100 ft/s airspeed at 6,500 ft and 95F. The fixed wing design's engine sizing condition is simply the steady power required at 100 ft/s and 6,500 ft, 95F. Table 5 presents the weight buildup for both aircraft designs. It can be readily observed that the battery weight is a substantial portion of the aircraft weight for both the ornithopter and the fixed wing, 43% and 45% of the aircraft gross weight, respectively. This highlights the potential for significant aircraft design improvement through enhancements in power and energy density of storage devices. Overall the fixed wing shows a 3.3% lower empty weight fraction, primarily due to the lower motor, wing and drive weights. Table 6 contains a summary of the design data for the two aircraft, including: wing, tail and body geometry, avionics power requirements and engine and battery sizes. Figure 22 shows a schematic of the ornithopter, providing overall dimensions.

Table 3. Ornithopter Design Mission Summary

Gross Weight, lb	12.0				
Payload, lb	0.3				
Battery, lb	4.9				
Battery Capacity, mAh	25,148				
Mission, mAh	19,052				
Reserve (10%), mAh	1,905				
Unusable (20%), mAh	4,191				
Segment	Climb	Cruise	Loiter	Cruise	Reserve
Distance, km	1.1	3.9	0.0	5.0	0.0
Time, min	0.8	2.6	90.0	3.3	10.9
Airspeed, ft/s	60	100	60	100	60
Rate of Climb, ft/min	594	0	0	0	0
Altitude, ft	6,000	6,500	6,500	6,500	6,500
Temperature, F	95	95	95	95	953
Power Required, W	241	241	97	241	97
Battery Capacity, mAh	222	1,133	16,404	1,293	1,905

Downloaded by UNIVERSITY OF COLORADO on January 11, 2017 | http://arc.aiaa.org | DOI: 10.2514/6.2017-0013

Table 4. Fixed Wing Design Mission Summary

Gross Weight, lb	8.5				
Payload, lb	0.3				
Battery, lb	3.9				
Battery Capacity, mAh	18,497				
Mission, mAh	14,013				
Reserve (10%), mAh	1,401				
Unusable (20%), mAh	3,083				
Segment	Climb	Cruise	Loiter	Cruise	Reserve
Distance, km	0.4	4.8	0.0	5.0	0.0
Time, min	0.4	3.1	90.0	3.3	18.6
Airspeed, ft/s	60	100	60	100	60
Rate of Climb, ft/min	1,423	0	0	0	0
Altitude, ft	6,000	6,500	6,500	6,500	6,500
Temperature, F	95	95	95	95	953
Power Required, W	226	226	61	226	61
Battery Capacity, mAh	130	1,162	11,543	1,217	1,403

Table 5. Component Weight Summary

	Ornithopter		Fixed Wing	
	lb	%GW	lb	%GW
Wing	2.32	19.3	1.58	18.5
Propeller	-	-	0.02	0.2
Tail	0.07	0.6	0.07	0.8
Body	1.53	12.8	1.21	14.1
Alighting Gear	0.05	0.4	0.05	0.6
Propulsion	1.27	10.6	0.26	3.1
Engine	0.23	1.9	0.11	1.3
ESC	0.33	2.7	0.15	1.8
Drive	0.71	5.9	-	-
Flight Controls	0.20	1.7	0.20	2.3
Instruments	0.05	0.4	0.05	0.6
Electrical	0.03	0.2	0.03	0.3
Avionics	0.68	5.6	0.68	7.9
Contingency	0.31	2.6	0.21	2.4
Empty Weight	6.50	54.2	4.34	50.9
Sensor (EO/IR)	0.33	2.7	0.33	3.8
Battery	5.17	43.1	3.87	45.3
Gross Weight	11.99	100.0	8.53	100.0

Downloaded by UNIVERSITY OF COLORADO on January 11, 2017 | http://arc.aiaa.org | DOI: 10.2514/6.2017-0013

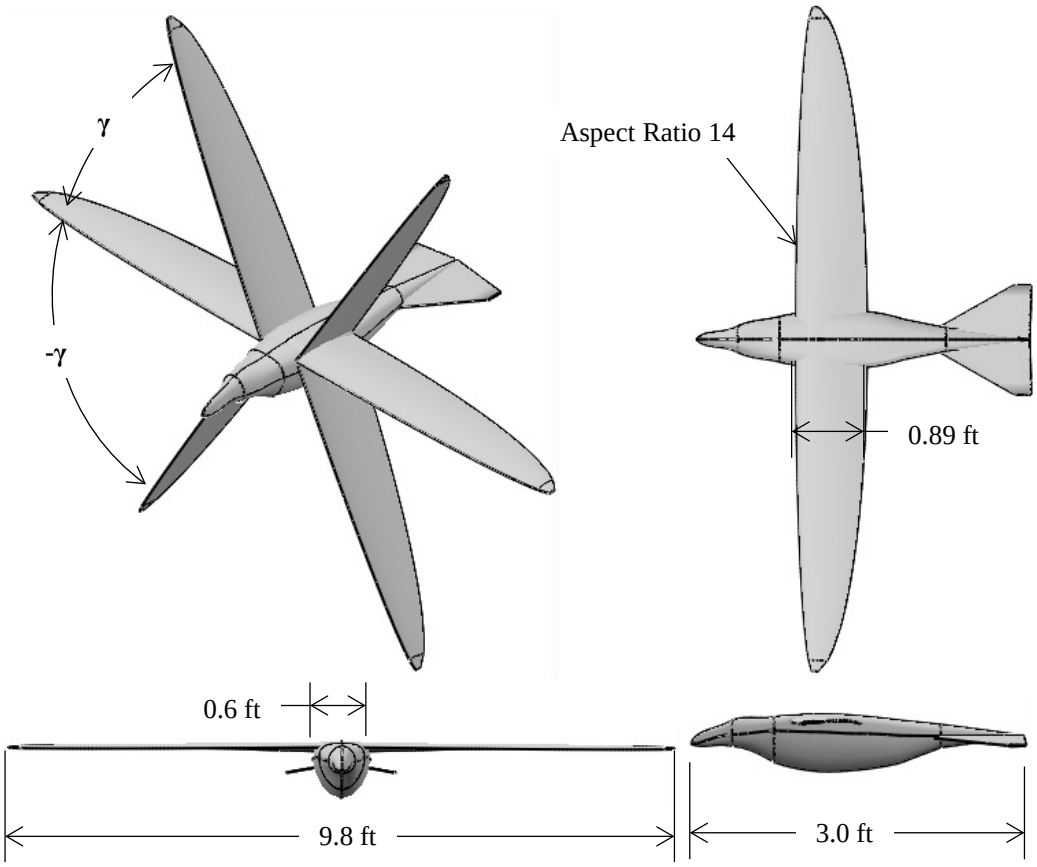

Figure 22. Ornithopter Sketch

While the fixed wing aircraft has an advantage in empty weight fraction and power losses, the ornithopter achieves a higher aerodynamic efficiency, as shown in Figure 23. For the mission considered in this study, this improved aerodynamic efficiency doesn't beat out the weight efficiency of the fixed wing design. However, considering the tradeoff between station time and range, shown in Figure 24, the ornithopter appears to have an advantage due to its higher aerodynamic efficiency. As to whether there exists a break-even point with respect to the cost function, further study is required.

Downloaded by UNIVERSITY OF COLORADO on January 11, 2017 | http://arc.aiaa.org | DOI: 10.2514/6.2017-0013

Downloaded by UNIVERSITY OF COLORADO on January 11, 2017 | http://arc.aiaa.org | DOI: 10.2514/6.2017-0013

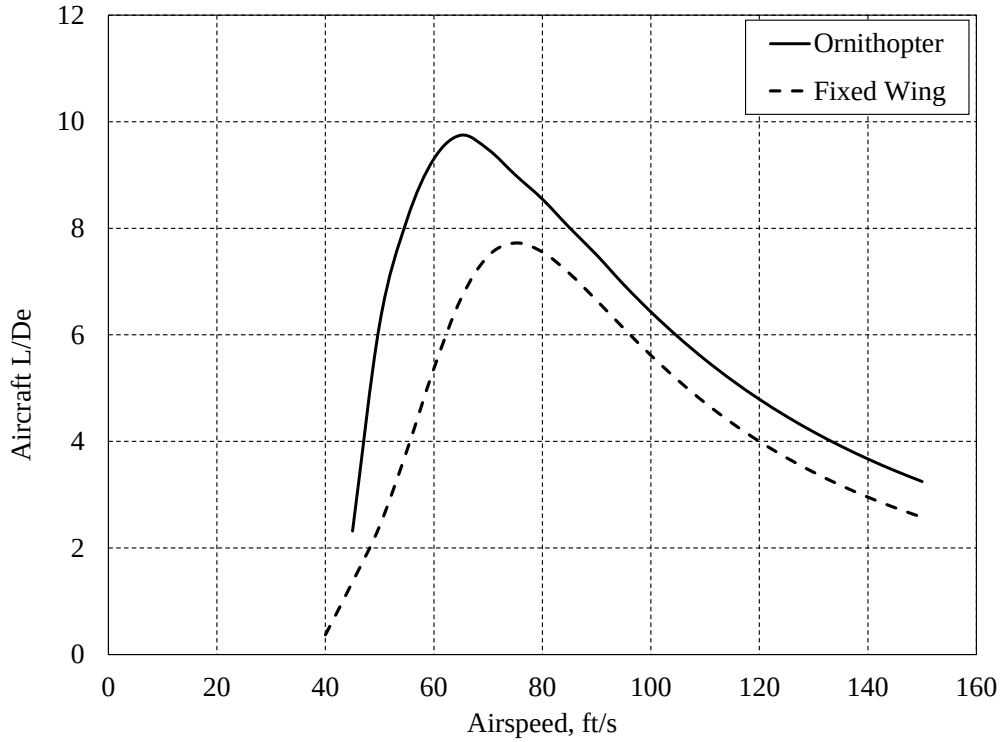

Figure 23. Aerodynamic Efficiency as a Function of Airspeed

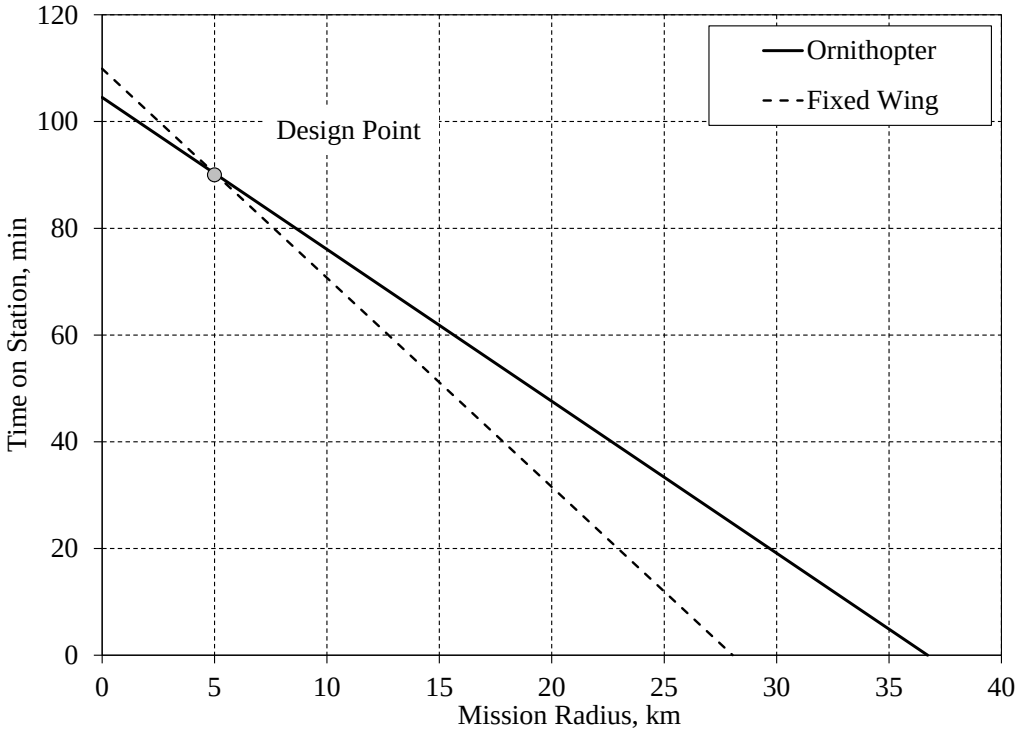

Figure 24. Time on Station as a Function of Mission Radius

IV. Conclusions

In this study it's observed that an ornithopter, within the size class considered, has improved aerodynamic efficiency when compared to a similar size fixed wing aircraft. This characteristic is offset by the increased weight of the wing to accomplish the motion and the driving mechanism. The net result, with respect to the cost function, is a 41% greater cost for the ornithopter. This large difference is dominated by the peak power requirement during the wing down stroke at the high speed cruise condition. Adding a spring or fly wheel to the mechanism may help to lower this penalty by reducing the peak to trough power requirements during the flap cycle.

Another interesting characteristic of the ornithopter, compared to the fixed wing, is its lower speed performance advantage. For the same wing loading, the ornithopter has 2 counts greater aerodynamic efficiency. The flapping, twisting and pitching motion of the wing delay the onset of stall as the airspeed is reduced. However, as Figs. 18-20 show, the range in wing gaits converge to a single feasible solution at an airspeed of 45 ft/s. Non-sinusoidal wing gaits may further improve the wing performance across the flight envelope, particularly if the wing can achieve its optimal steady flap rate for longer portions of the flap arc. Mechanizing this desired motion will likely require increased complexity in the drive mechanism, compared to the relatively simple sinusoidal mechanisms.

This study demonstrates that the ornithopter is a viable configuration in the man-portable size class of UAS. While the current study showed higher cost, as anticipated, the improved aerodynamic efficiency compared to a fixed wing could prove beneficial for a different mission. Additional study of various wing gaits, beyond sinusoidal motion, could yield improved aerodynamic efficiency and controlled flight at lower airspeeds, approaching hover. The potential capabilities the ornithopter brings, beyond fixed and rotary wing aircraft, warrants further exploration of this concept.

V. References

1. Shyy W., Lian Y., Tang J., Liu H., Trizila P., Stanford B., Bernal L., Cesnik C., Friedmann P., Ifju P., "Computational aerodynamics of low Reynolds number plunging, pitching and flexible wings for MAV applications," Acta Mechanica Sinica, vol. 24(4), pp. 351-373, August 1, 2008.
2. Hein, B. R., Chopra, I., "Hover performance of a micro air vehicle: rotors at low Reynolds number." Journal of the American Helicopter Society, vol. 52.3, pp. 254-262, 2007.
3. Ananthanarayanan, A., Gupta, S. K., Bruck, H. A., "Characterization and control of plastic deformation in mesoscale premolded components to realize in-mold assembled mesoscale revolute joints," Polymer Engineering & Science, vol. 49(2), pp. 293-304, 2009.
4. Singh, B., Chopra, I., "Insect-based hover-capable flapping wings for micro air vehicles: experiments and analysis," AIAA journal, vol. 46(9), pp. 2115-2135, 2008.
5. Keennon M, Klingebiel K, Won H, Andriukov A. "Development of the nano hummingbird: A tailless flapping wing micro air vehicle," AIAA Aerospace Sciences Meeting, January 12, 2012, Reston, VA.
6. Roget, B., Sitaraman, J., Harmon, R., Grauer, J., Hubbard, J., & Humbert, S., "Computational study of flexible wing ornithopter flight," Journal of Aircraft, vol. 46(6), pp. 2016-2031, 2009.
7. Grauer, J. A., & Hubbard, J. E., "Multibody model of an ornithopter. Journal of guidance, control, and dynamics," vol. 32(5), pp. 1675-1679 2009.
8. Hubbard, J. E., Frecker, M. I., "Design, Fabrication and Testing of a Passively Morphing Ornithopter Wing for Increased Lift and Agility," AFOSR Final Technical Report, FA9550-09-1-0632, December 2012.
9. Send, W., Fischer, M., Jebens, K., Mugrauer, R., Nagarathinam, A., Scharstein, F., "Artificial hinged-wing bird with active torsion and partially linear kinematics," 28th Congress of the International Council of the Aeronautical Sciences, pp. 23-28, September 2012.
10. Mackenzie, D., "A flapping of wings," Science, vol. 335(6075), pp. 1430-1433, 2012.
11. Klavdianos, D., "Aeria Bird Repelling System. From lab to the landing strip. From the FESTO SmartBird towards a viable product against bird strikes," Doctoral dissertation, Delft University of Technology, 2014.
12. Räbiger, H., "Wie Ornithopter fliegen, Aerodynamik und Dynamik großer Schlagflügelmodelle," Self-published, Nuremberg, Germany, 2001.

Downloaded by UNIVERSITY OF COLORADO on January 11, 2017 | http://arc.aiaa.org | DOI: 10.2514/6.2017-0013

13. Räbiger H., “Arrangements of wing tip vortices on flapping wings,” Flapping Wings Newsletter, Winter Issue, 2015.

14. Tobalske, B. W., Dial, K. P., “Flight Kinematics of Black-Billed Magpies and Pigeons Over a Wide Range of Speeds,” Journal of Experimental Biology, 199, 263-280, 1996.

15. Rayner, J. M., “Estimating Power Curves of Flying Vertebrates,” Journal of Experimental Biology, 202, 3449-3461, 1999.

16. Tobalske, B. W., “Biomechanics of Bird Flight,” Journal of Experimental Biology, 210, 3135-3146, 2007.

17. Usherwood, J. R., “The Aerodynamic Forces and Pressure Distribution of a Revolving Pigeon Wing,” Journal of Experimental Fluids, 46(5), 991-1003, May 2009.

18. DeLaurier, James D. “An aerodynamic model for flapping-wing flight,” Aeronautical Journal 97.964 (1993): 125-130.

19. Kim, D. K., Lee, J. S., Han, J. H., “Improved Aerodynamic Model for Efficient Analysis of Flapping-Wing Flight,” AIAA Journal, Vol. 49, No. 4, April 2011.

20. Parslew, B., Crowther, W. J., “Simulating avian wingbeat kinematics,” Journal of Biomechanics, 43(16), pp. 3191-3198, 2010.

21. U.S. Army, “Unmanned aircraft systems roadmap 2010–2035,” US Army UAS Center of Excellence, Fort Rucker, AL, 2010.

22. Beekman, D. W., Mait, J. N., and Doligalski, T. L., “Micro Autonomous Systems and Technology at the Army Research Laboratory,” Proc. NAECON (2008).

23. International Society of Allied Weight Engineers, Inc., Recommended Practice Number 8, June 1, 1997.

24. Johnson, W., “NDARC - NASA Design and Analysis of Rotorcraft. Theoretical Basis and Architecture,” American Helicopter Society Aeromechanics Specialist’s Conference Proceedings, San Francisco, CA, Jan. 20–22, 2010.

25. Anderson, J. D., Fundamentals of Aerodynamics. Boston: McGraw-Hill, 2001.

26. Williamson, G.A., McGranahan, B.D., Broughton, B.A., Deters, R.W., Brandt, J.B., and Selig, M.S., “Summary of Low Speed Airfoil Data, Volume 5,” Department of Aerospace Engineering, University of Illinois at Urbana-Champaign, 2012.

27. Brandt, J.B. and Selig, M.S., “Propeller performance data at low Reynolds numbers,” 49th AIAA aerospace sciences meeting, 2011-1255, January 2011.

28. Harris, F.D., and Scully, M.P. “Rotorcraft Cost Too Much.” Journal of the American Helicopter Society, Vol. 43, No. 1, January 1998.

Downloaded by UNIVERSITY OF COLORADO on January 11, 2017 | http://arc.aiaa.org | DOI: 10.2514/6.2017-0013